the alloys with Cr contents in the range 17.3 to 25.5 wt.% developed Cr_2O_3 and (Fe,Cr) oxide spinel. The Raman spectra for surface carbon in these alloys are also similar but vary in the relative peak height for the D and G bands. Figures 48 and 49 show the Raman spectra in the frequency ranges of 200-800 cm^{-1} and 1200-1800 cm^{-1}, respectively, for several alloys with varying Al content. Even though the Al content of alloys MA956 and APMT is similar, their scaling behavior is somewhat different. Alloy APMT predominantly developed Cr_2O_3 scale, as evidenced by the sharp peak at ≈550 cm^{-1}, whereas the alloy MA956 (which exhibited a much thinner scale) showed a less developed peak at a frequency >550 cm^{-1}. The peak at ≈700 cm^{-1} in the APMT alloy is not presently identified, except that it does not correspond to any Al_2O_3 phase. Even in the higher frequency range (that corresponding to carbon, see Fig. 49), the relative intensities for the D-to-G band for the two alloys are different, but the cause for it is not known. The Raman spectra for the alloys 602CA and 214 (with a lower Al content) are similar in the entire frequency range.

Figures 50 and 51 show the Raman spectra in the frequency ranges of 200-800 cm^{-1} and 1200-1800 cm^{-1}, respectively, for several alloys with varying Si content. The alloys selected for these figures (253MA, 38815, 45TM, and HR160) contain 13.9-28.0 wt.% Cr and 1.6-5.8 wt.% Si. The results showed that all four alloys developed predominantly Cr_2O_3 scale, which is expected based on oxidation studies of Si-containing alloys. In general, Si can form a silica scale at the Cr_2O_3/alloy interface since the diffusion coefficient for Si is much smaller than that for either Cr or Fe, and these alloys can rarely form an external scale of silica at the Si concentration levels present in these alloys. The Raman spectra in the frequency range of 1200-1800 cm^{-1} show similar peaks on all four alloys, indicating that the variation in Si content in these alloys has virtually no effect on the deposition of carbon.

DISCUSSION OF METAL DUSTING INITIATION

The results presented thus far clearly indicate that the gas chemistry used in Runs 15 and 16 can deposit carbon by the reactions that were discussed earlier. Furthermore, decreasing the H_2O content of the gas, thereby increasing the carbon activity (e.g., Run 19), can accelerate carbon deposition. However, whether the deposited carbon can initiate metal dusting in Fe- and Ni-base alloys is strongly influenced by the oxidation characteristics of the alloys. The competition between the oxidation process to form a continuous oxide scale on a given alloy surface and deposition and penetration of carbon will determine the incubation time for metal dusting attack to occur. If an alloy can develop a protective oxide scale fast enough and early during exposure, then subsequent deposition of carbon on top of the oxide layer can delay initiation of metal dusting.

In most earlier studies on metal dusting, the researchers selected gas compositions that yielded carbon activities >>1, which led to deposition of carbon on the specimens from

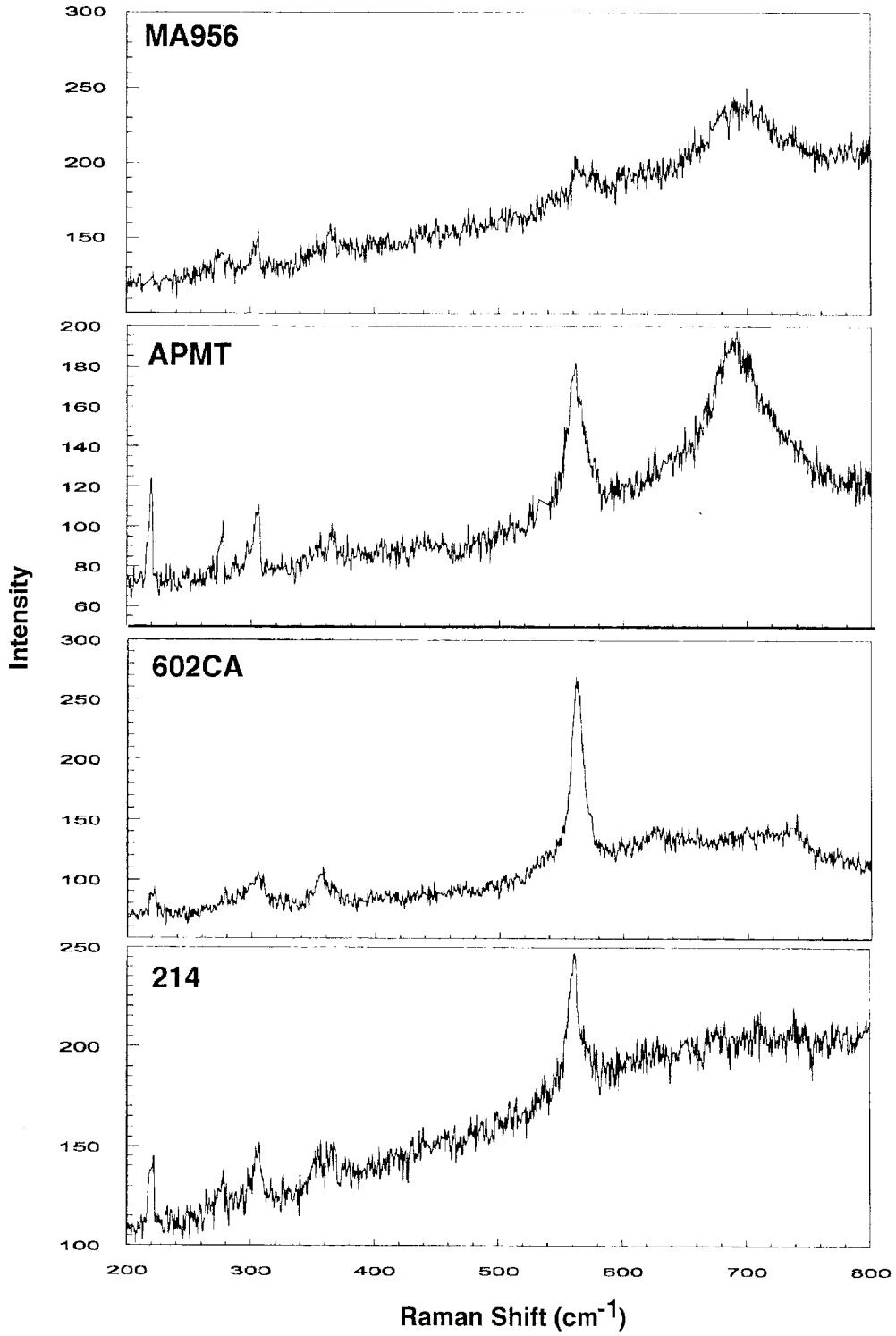

Fig. 48. Raman spectra (frequency range 200-800 cm^{-1}) for surfaces of several Al-containing alloys (MA956, 4.5 wt.%; APMT, 4.9 wt.%; 602CA, 2.3 wt.%; and 214, 3.7 wt.%) after 1000-h exposure in a metal dusting environment at 593°C (1100°F).

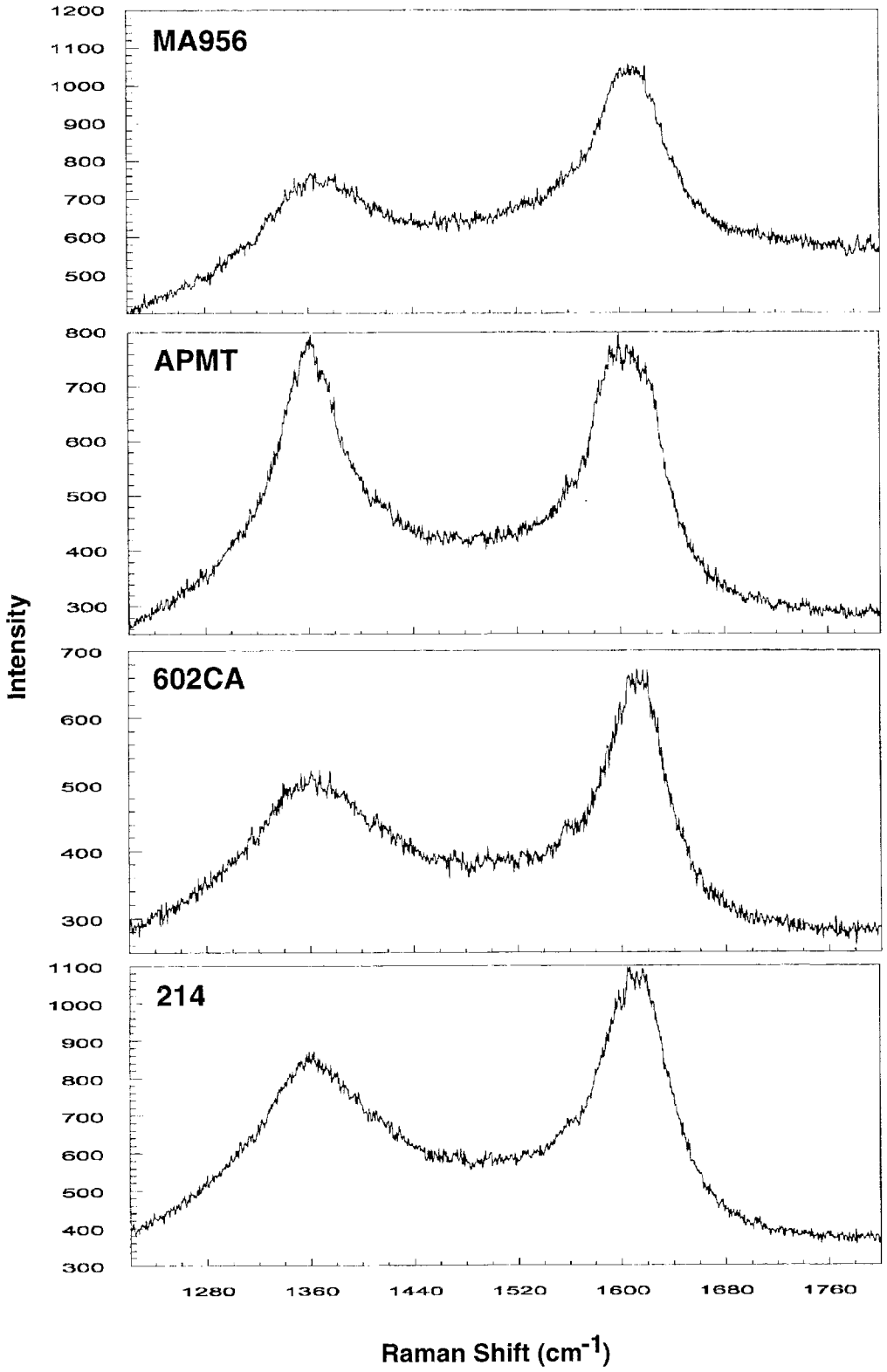

Fig. 49. Raman spectra (frequency range 1200-1800 cm^{-1}) for surfaces of several Al-containing alloys (MA956, 4.5 wt.%; APMT, 4.9 wt.%; 602CA, 2.3 wt.%; and 214, 3.7 wt.%) after 1000-h exposure in a metal dusting environment at 593°C (1100°F).

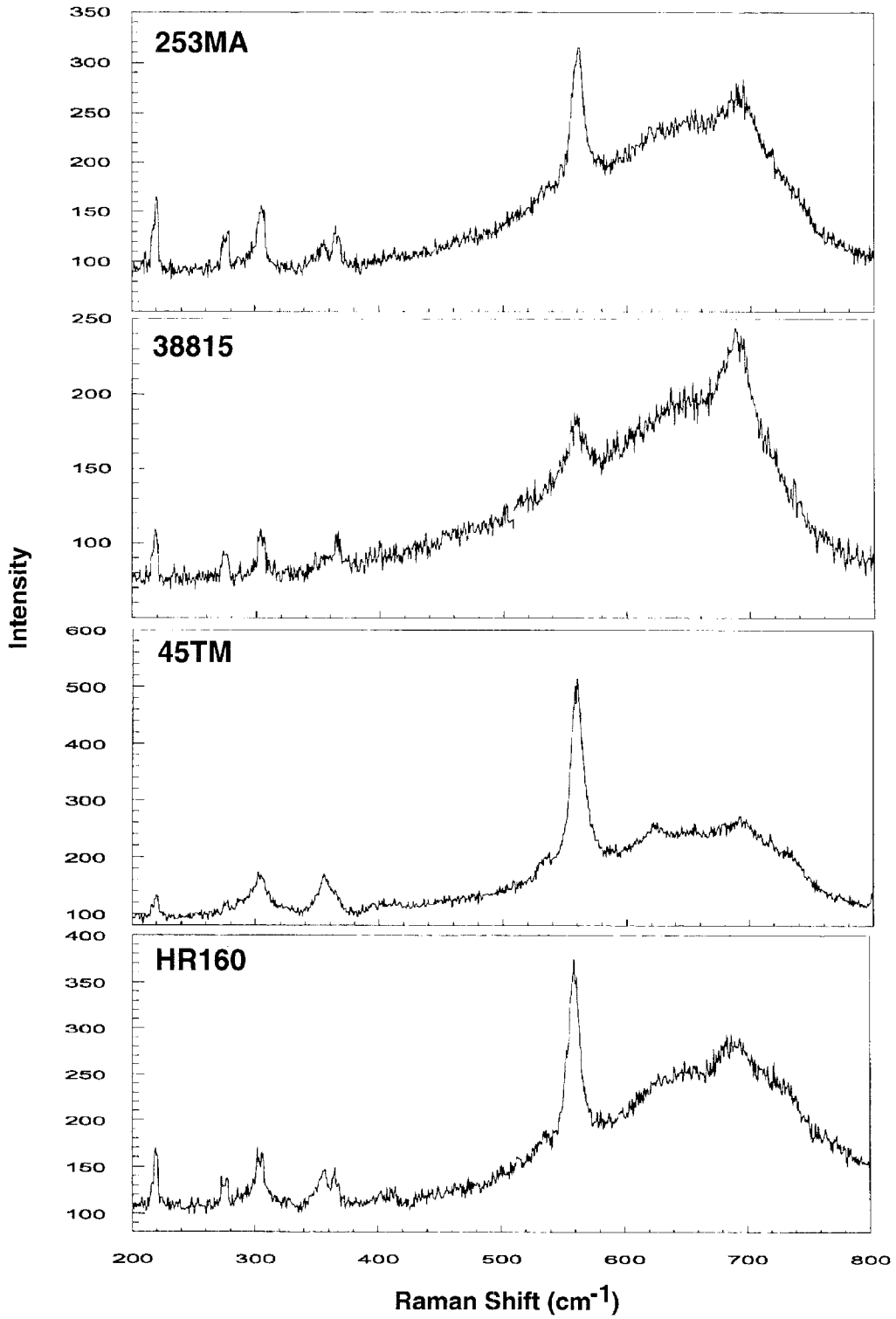

Fig. 50. Raman spectra (frequency range 200-800 cm^{-1}) for surfaces of several Si-containing alloys (253MA, 1.6 wt.%; 38815, 5.8 wt.%; 45TM, 2.7 wt.%; and HR160, 2.8 wt.%) after 1000-h exposure in a metal dusting environment at 593°C (1100°F).

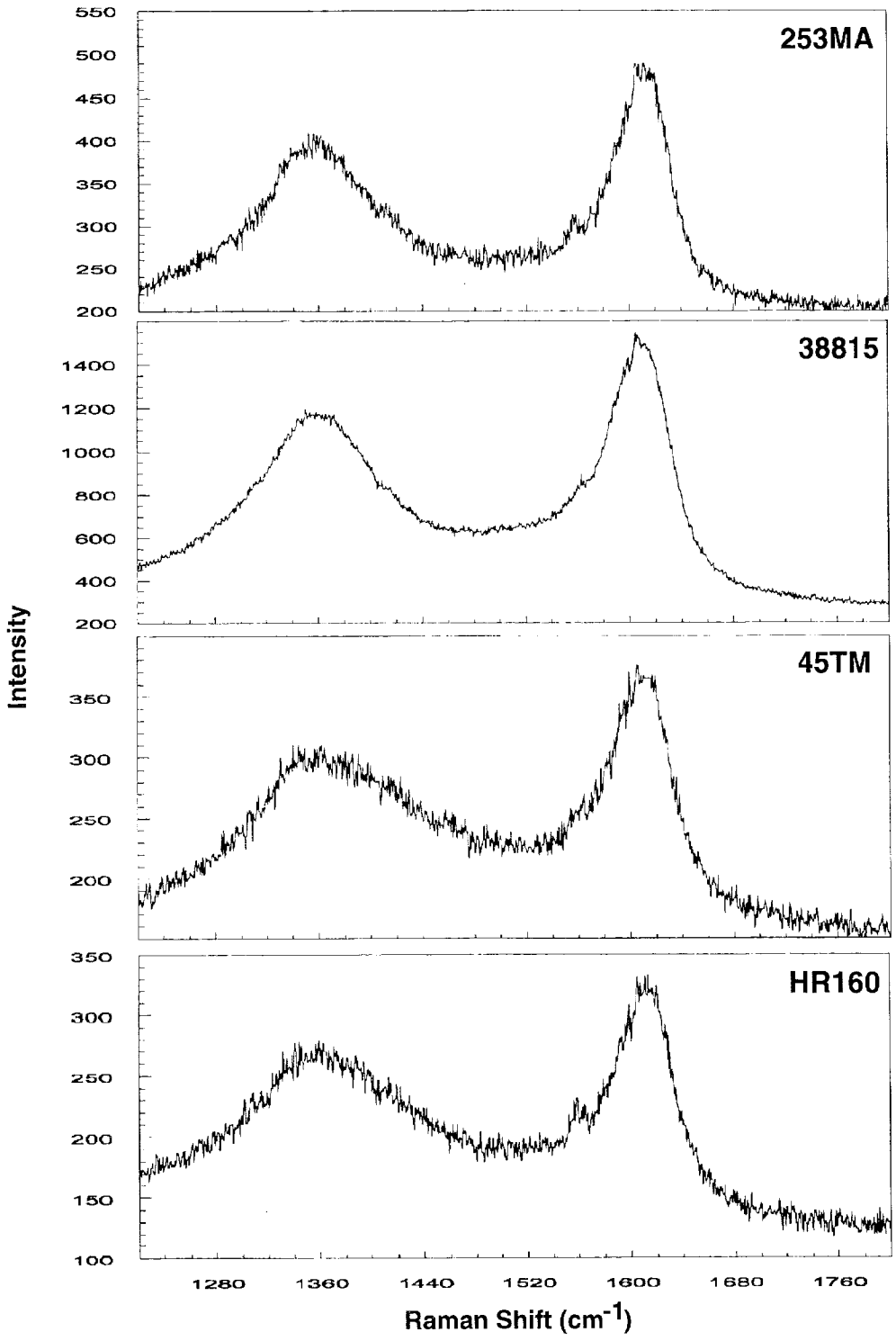

Fig. 51. Raman spectra (frequency range 1200-1800 cm^{-1}) for surfaces of several Si-containing alloys (253MA, 1.6 wt.%; 38815, 5.8 wt.%; 45TM, 2.7 wt.%; and HR160, 2.8 wt.%) after 1000-h exposure in a metal dusting environment at 593°C (1100°F).

the beginning of the exposure.[9,30-32] Besides exposure to high carbon activity, the alloys did not have much time (before carbon deposition) to develop a protective oxide scale. Therefore, the earlier studies emphasized interaction of the deposited carbon with the constituents of the structural alloys and examined the role of alloy-related variables (such as alloy composition; Fe, Cr, and Ni contents; surface preparation; and surface roughness) on alloy degradation. A comparative analysis was conducted on the carbon activities and oxygen partial pressures established in several studies to better understand the role of gas chemistry in the metal dusting behavior of structural alloys.

Table 6 lists the chemical compositions of gases used in several of the studies. The H_2O content in the past studies was in the range 0-2.4 vol.%, whereas we used H_2O contents of 0, 2, and 23 vol.% (the last one is typical of the effluent from a H_2 reformer). Similar to results presented in an earlier section in this report, we calculated the carbon activity of various gas mixtures at several temperatures in the range of 425-760°C (800-1400°F).

Table 6. Gas chemistries used in metal dusting research

	Composition in vol. %				
Researcher	CO	CO_2	CH_4	H_2	H_2O
Grabke (Ref. 9)	24.7	-	-	73.4	1.9
Maier et al. (Ref. 31)	24.4	-	-	73.2	2.4
Baker/Smith (Ref. 32)	70.0	4.0	-	25.3	0.75
Levi et al. (Ref. 33)	25.0	-	-	75.0	-
Natesan et al. (gas 4)	17.5	8.3	-	74.2	-
Natesan et al. (gas 5)	17.6	8.3	-	72.2	2.0
Natesan et al. (gas 2)	18.0	5.6	1.1	52.0	23.0

Table 7 lists the carbon activity values at 593°C (1100°F) calculated for gas mixtures used in past studies and the current program. The calculations are based on whether Reaction 1 or 2 was dominant or equilibrium between different gas species prevailed at the elevated temperature. The carbon activities in past studies have been >>1, irrespective of whether Reaction 1 or 2 dominated the process. If the gases were in thermodynamic equilibrium, the carbon activity in most cases is around 1. A carbon activity value of infinity under the Reaction 1 column (in Table 7) arises because the inlet gas mixture in the study did not contain H_2O, whereas infinity under Reaction 2 arises because the mixture did not contain CO_2. The calculated carbon activity values are based on initial gas compositions. Once Reaction 1 starts, H_2O will be generated, and the local carbon activity will be less than the calculated values in Table 7. However, carbon deposition would have occurred, and it would be almost impossible to develop a protective oxide scale on the alloy surface.

Table 7. Carbon activity and oxygen partial pressure values at 593°C (1100°F), for gas mixtures used by various researchers

Researcher	Carbon activity			Oxygen pressure (in atm), based on		
	Rxn 1	Rxn 2	Eqm	CO/CO_2	H_2/H_2O	Eqm
Grabke (Ref. 9)	47.5	∞	1.2	-	6.7×10^{-28}	7.6×10^{-26}
Maier et al. (Ref. 31)	37.1	∞	1.2	-	1.1×10^{-27}	7.7×10^{-26}
Baker/Smith (Ref. 32)	118.0	165.0	0.8	3.1×10^{-28}	1.0×10^{-28}	3.9×10^{-25}
Levi et al. (Ref. 33)	∞	∞	1.2	-	-	6.9×10^{-26}
Natesan et al. (gas 4)	∞	5.0	1.3	2.2×10^{-26}	-	1.1×10^{-25}
Natesan et al. (gas 5)	32.5	5.0	1.2	2.2×10^{-26}	7.6×10^{-28}	1.2×10^{-25}
Natesan et al. (gas 2)	2.0	7.9	0.7	9.5×10^{-27}	1.2×10^{-25}	2.4×10^{-25}

Table 7 also lists the oxygen partial pressure (pO_2) values at 593°C (1100°F), calculated for three possible assumptions: CO/CO_2 or H_2/H_2O ratio determines the pO_2, or a thermodynamic equilibrium exists between all the gaseous species at the elevated temperature. The calculations indicate that for a given gas composition, the equilibrium pO_2 values are always higher than those established by either CO/CO_2 or H_2/H_2O ratios. If one assumes that the gas composition does not change significantly during flow from the exit of the reformer to low temperature sections of the waste-heat boiler (i.e., the carbon deposition reactions are slow enough that the generation of carbon by catalysis of gas phase constituents causes little change in bulk gas chemistry), then the pO_2 in the environment will be dictated by the higher of the two values calculated from CO/CO_2 and H_2/H_2O ratios.

From the materials standpoint one can analyze the type of interactions between the constituents of the alloy and the environment by means of thermochemical diagrams. Since carbon deposition and formation of the oxide layer on the metal surface are of interest for materials exposed to metal dusting environments, oxygen/carbon diagrams were generated for several temperatures in the range of 400-700°C. Figure 52 shows the oxygen/carbon thermochemical diagrams for Fe, Cr, and Ni calculated for 593°C. The diagrams depict the stability fields for the metals, oxides, and carbides of Fe, Cr, and Ni in terms of carbon and oxygen partial pressures. Superimposed on these diagrams (indicated by boxes) are the oxygen and carbon partial pressure ranges for gas mixtures used by various researchers in metal dusting studies. The calculations show that Fe_3C, Cr_2O_3, Ni, and Ni_3C are the phases that will be stable in the environments used in the laboratory research and in gas mixtures corresponding to the effluent of the H_2 reformer (Gas 2).

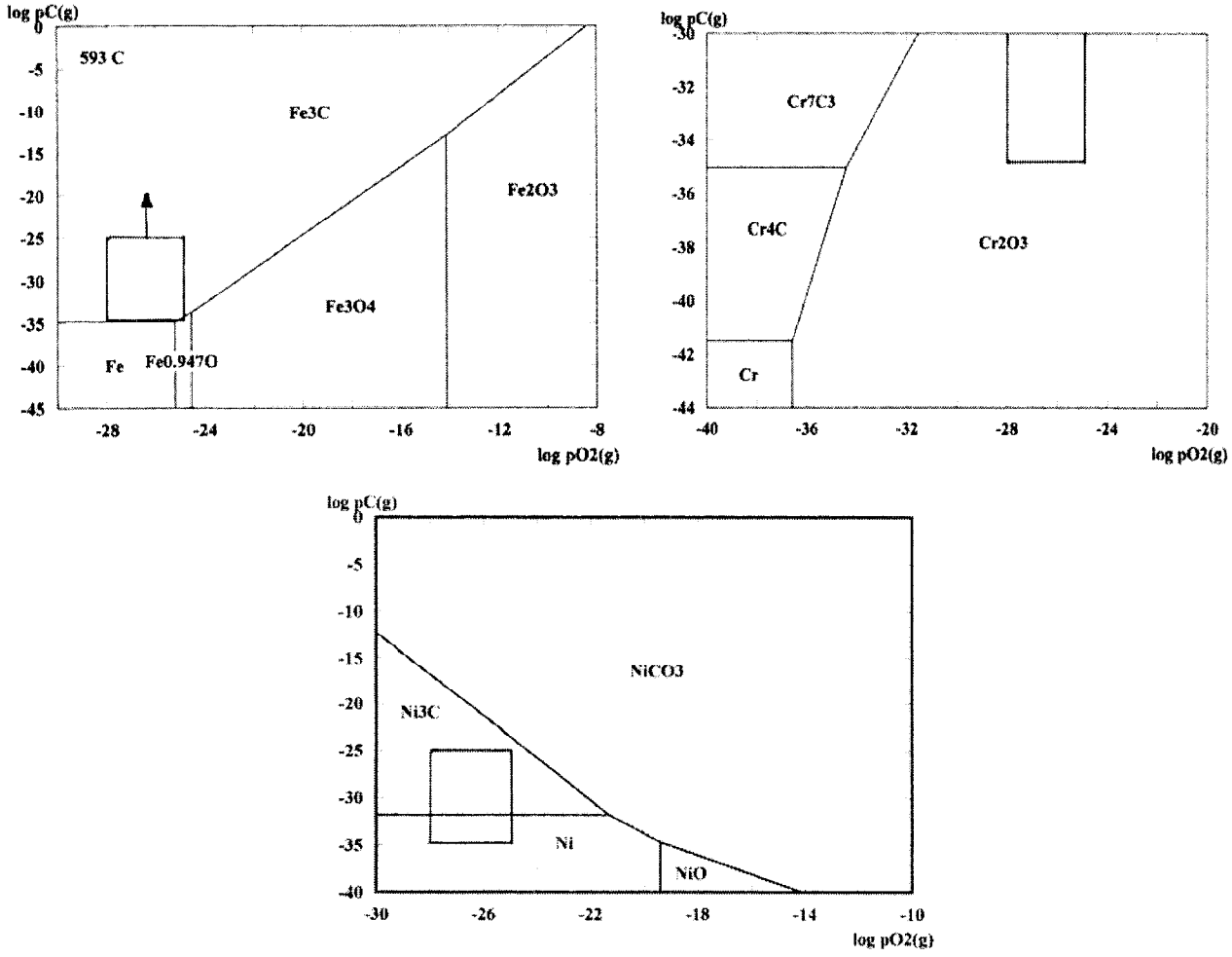

Fig. 52. Oxygen/carbon thermochemical diagrams for Fe, Cr, and Ni calculated for 593°C (1100°F).

For pure Fe and for Fe-base alloys containing low concentrations of Cr (e.g, T22), the calculations indicate that Fe_3C would be the primary phase that forms upon exposure to the metal dusting environment. This observation has been validated by experimental results reported earlier in this report (see Fig. 14 for example). In the case of high-Cr alloys of both Fe- and Ni-base types, pure Cr oxide or Cr-rich oxide will be the stable phase that form upon exposure of the alloy to metal dusting environments, unless precipitous deposition of carbon occurs from the beginning of exposure such that the alloy surface is completely covered with carbon and no time is available to develop an oxide scale. We believe such was the case in most of the earlier studies, which had a_C >>1 and extremely low H_2O content. In Runs 15 and 16 conducted at ANL, the H_2O content of Gas Mixture 2 was 23 vol.%, and a_C was somewhat greater than 1. For this condition, the alloys exhibited oxide scales with subsequent deposition of carbon on top of the oxide.

In reformers, the metal dusting attack generally occurs over a period of years of service, while in laboratory studies the attack occurs over a period of a few hours to few days. Thus, in the reformer, the degradation process is dictated by the breakdown of the oxide scale, while in the laboratory studies, the attack begins right from the start. The ANL program will simulate the environments that are prevalent in reformer systems and examine the competition between the oxide scale development and its breakdown leading to metal dusting attack. Therefore, an understanding of the incubation period and initiation time for metal dusting morphology (such as surface pits) will be emphasized.

PERFORMANCE OF PACK-DIFFUSION COATINGS

Coatings can minimize gas phase reactions by lack of availability of metal surfaces for catalysis. This, in turn, can minimize or eliminate coking and carbon deposition. Furthermore, coatings can act as barriers to carbon ingress into the substrate alloy since carbon diffusion through oxide scales is generally orders of magnitude lower than through the alloys. Among the oxides, the potential candidates as coatings are chromia, alumina, and silica. Iron oxide may not be a viable candidate unless the oxide-to-carbide reaction is slow enough that oxide can be maintained for the desired service life.

Three approaches are being examined for the development of oxide surface layers for evaluation in metal dusting environments. The first approach is to develop the oxide layer on the structural alloys by a preoxidation treatment. In this case, the specimens are exposed to either air or a low-pO_2 (established by H_2/H_2O or CO/CO_2 gas mixtures) environment at temperatures between 750 and 900°C. Generally, depending on the Cr content of the alloy and pO_2 in the exposure environment, the alloys develop (Fe,Cr) or (Ni,Cr) spinels or "pure" Cr oxide on the surface. Regulating the exposure time and temperature can control the thickness of the oxide layer.

The second approach involves a pack-diffusion process in which the alloy surface is enriched in oxide-forming elements such as Al, Cr, and/or Si. Subsequently, the surface-enriched alloy is oxidized in air to develop the oxide scale of choice. Pack diffusion is widely used to confer oxidation resistance on ferrous alloys. Pack diffusion processes include aluminizing, chromizing, and siliconizing. Specimens/components are packed in metal powders in sealed heat-resistant retorts and heated inside a furnace to precisely controlled temperature-time profiles. In the aluminizing process, a source of Al reacts with a chemical activator on heating to form a gaseous compound (e.g., pure Al with NaF to form AlF). This gas is the transfer medium that carries aluminum to the component surface. The gas decomposes at the substrate surface, depositing Al and releasing the halogen activator. The halogen activator returns to the pack and reacts with the Al again. Thus, the transfer process continues until all of the aluminum in the pack is used or until the process is stopped. The coating forms at temperatures ranging from 700 to 1100°C over a period of several hours.

Specimens with Al (termed "alonizing") and Cr/Si (termed "ChromePlexing") enrichment were obtained from Alon Surfaces for evaluation in metal dusting environments. Substrates selected for Al enrichment included three Fe-base alloys (T22, 800, and 321 stainless steel) and three Ni-base alloys (601, 625, and HR160). Substrates selected for ChromePlexing included only the three Fe-base alloys since it was not feasible to enrich Cr/Si on Ni-base alloys.

The third approach is thermal spraying. This surface treatment involves injecting energy into the surface of the work piece so that adhesion can take place. Conventional surface finishing methods involve heating an entire component, but the thermal spray technique usually adds energy and material into the surface, keeping the bulk of the object relatively cool and unchanged. This allows surface properties to be modified with minimal effect on the structure and properties of the underlying material. Coatings can be sprayed from rod or wire stock or from powdered materials. The material (e.g., wire) is fed into a flame, where it is melted. The molten stock is then stripped from the end of the wire and atomized by a high velocity stream of compressed air or other gas, which propels the material onto a prepared substrate or workpiece. The basic steps involved in any thermal coating process are substrate preparation, masking and fixturing, coating, finishing, inspection, and stripping (if necessary). Roughening is necessary for most of the thermal spray processes to ensure adequate bonding of the coating to the substrate. Specimens with a thermal spray coating of FeAl are included for evaluation in metal dusting environments.

Figures 53-55 show SEM photomicrographs of cross sections of alonized Fe-base alloys (T22, 321 stainless steel, and Alloy 800) along with elemental profiles as a function of coating thickness obtained by EDX analysis. The aluminum concentration at the surface of all three alloys in the as-coated condition was in a range of 35-45 wt.%. The depth profile in T22 shows a gradual decrease in Al concentration to a depth of ≈300 μm. The aluminum concentration profile in 321 stainless steel (which contains ≈10.3 wt% Ni) is less gradual, but the depth of Al-enriched layer is ≈200 μm. In Alloy 800 (which contains 31.7 wt.% Ni) a layer of Ni_3Al intermetallic forms on the interface between the Al enriched layer and the alloy substrate. This layer seems to slow the diffusion of Al into the substrate, with the result that the Al concentration profile is much flatter (28-36 wt.% Al) over a distance of 140 μm, after which the Al concentration drops sharply.

Figures 56-58 show SEM photomicrographs of cross sections of ChromePlexed Fe-base alloys (T22, 321 stainless steel, and Alloy 800) along with elemental profiles as a function of coating thickness obtained by EDX analysis. Chromium and silicon concentrations at the surface of T22 steel were 12 and 2.5 wt.%, respectively. The elemental profiles show that these concentrations remain fairly constant up to a depth

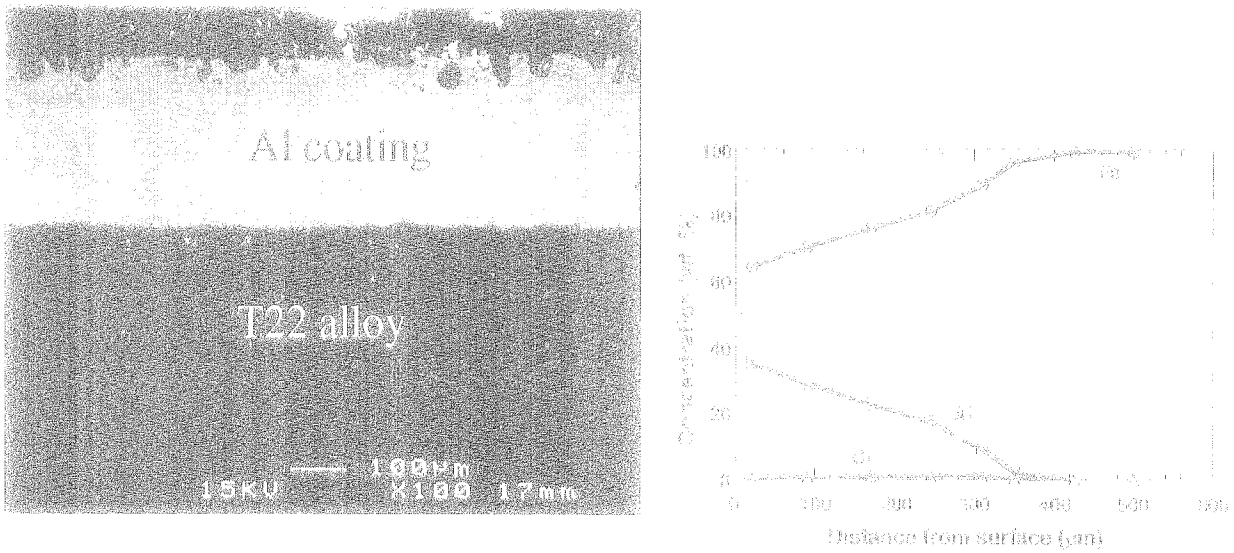

Fig. 53. SEM photomicrograph of cross section of aluminized T22 steel and EDX elemental depth profiles of Al and Fe for the specimen in the as-coated condition.

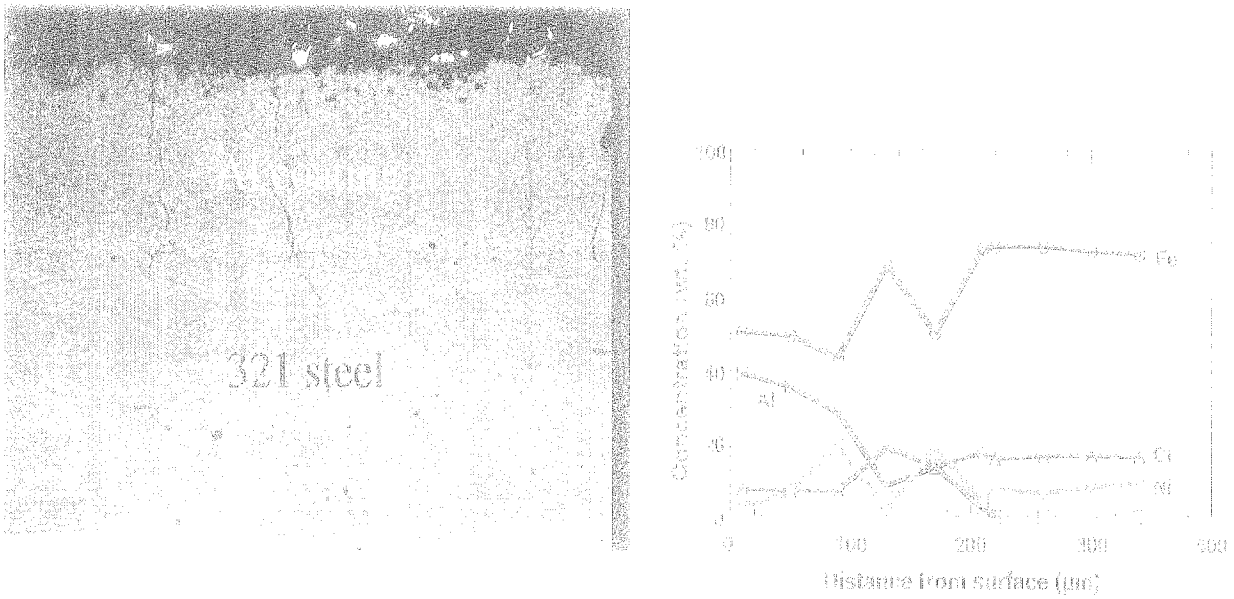

Fig. 54. SEM photomicrograph of cross section of aluminized 321 stainless steel and EDX elemental depth profiles of Al, Fe, Cr, and Ni for the specimen in the as-coated condition.

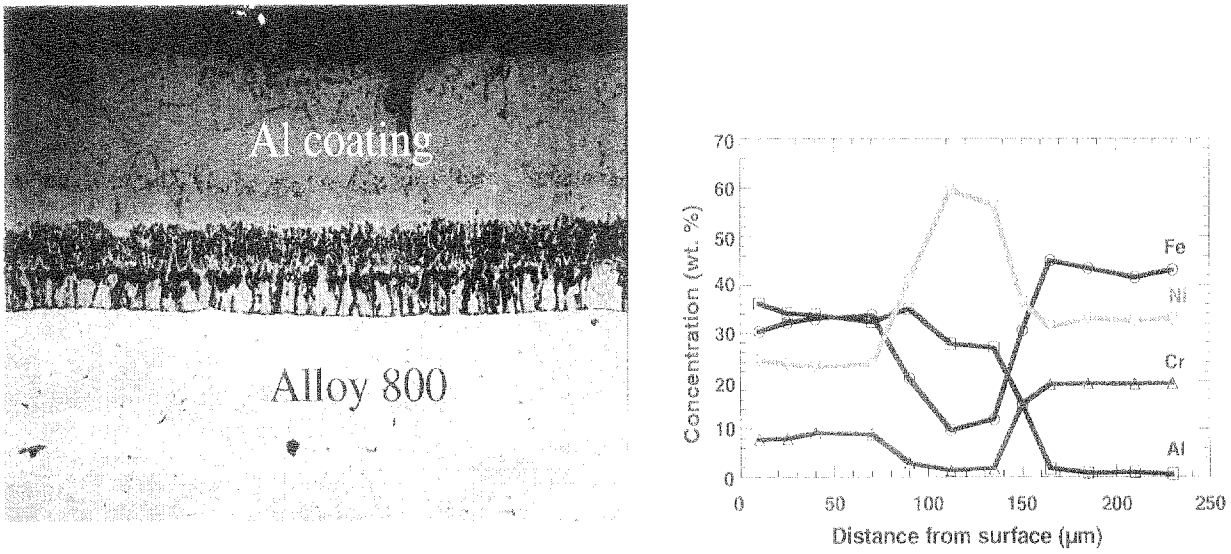

Fig. 55. SEM photomicrograph of cross section of alonized Alloy 800 and EDX elemental depth profiles of Al, Fe, Cr, and Ni for the specimen in the as-coated condition.

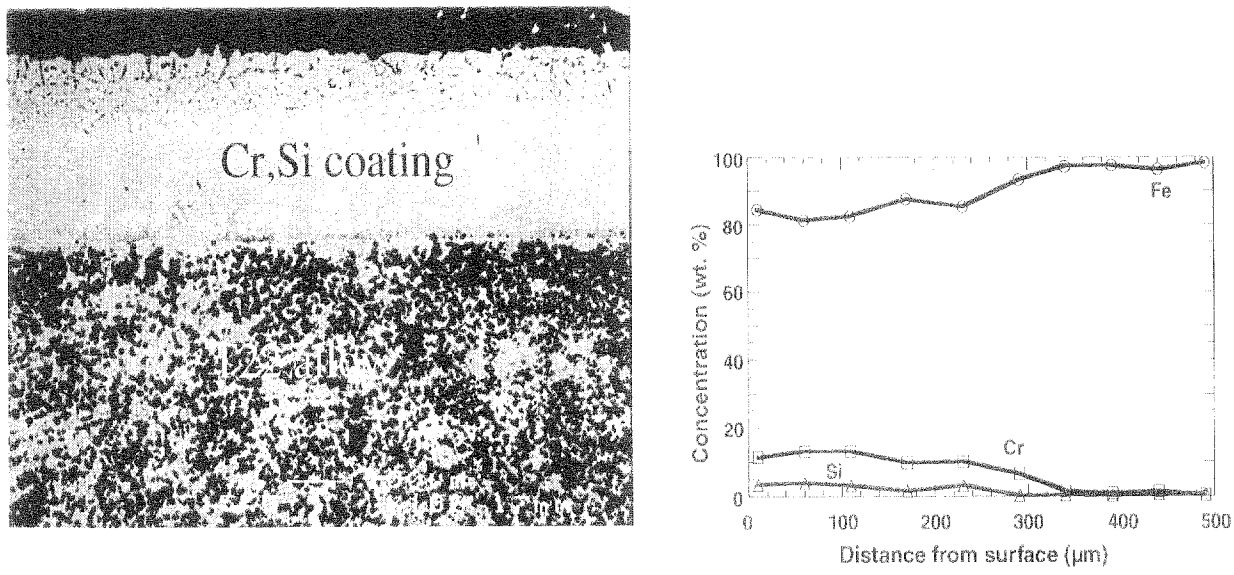

Fig. 56. SEM photomicrograph of cross section of ChromePlexed T22 steel and EDX elemental depth profiles of Si, Fe, and Cr for the specimen in the as-coated condition.

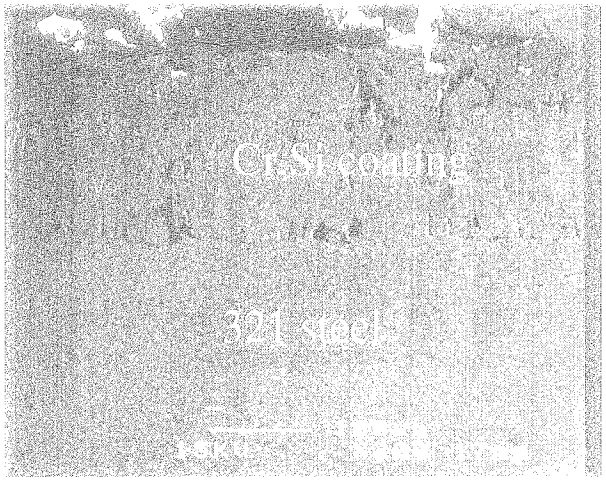

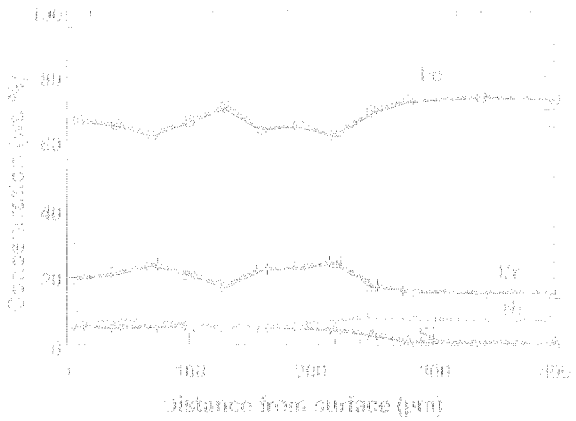

Fig. 57 – SEM photomicrograph of cross section of ChromePlexed 321 stainless steel and EDX elemental depth profiles of Si, Fe, Cr, and Ni for the specimen in the as-coated condition.

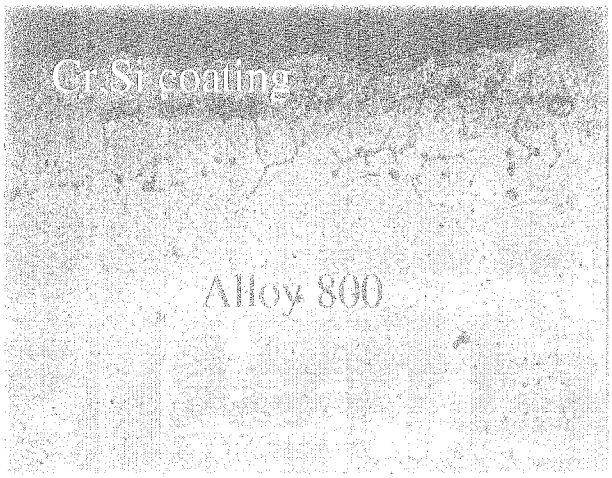

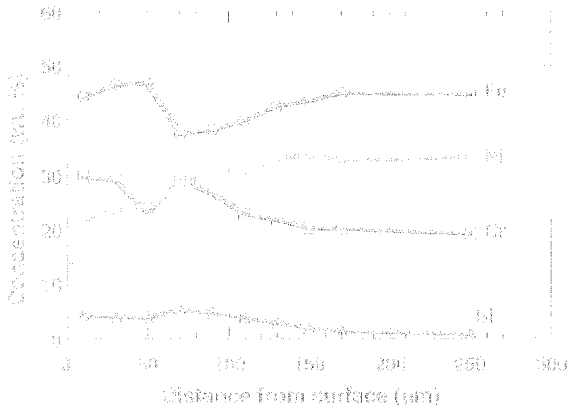

Fig. 58 – SEM photomicrograph of cross section of ChromePlexed Alloy 800 and EDX elemental depth profiles of Si, Fe, Cr, and Ni for the specimen in the as-coated condition.